

Article

Effects of Environmental Relative Vorticity and Seasonal Variation on Tropical Cyclones over the Western North Pacific

Yusi Wu ¹, Shumin Chen ^{1,*}, Mingsen Zhou ², Yilun Chen ¹, Aoqi Zhang ¹, Chaoyong Tu ¹ and Weibiao Li ¹

¹ Southern Marine Science and Engineering Guangdong Laboratory (Zhuhai), School of Atmospheric Sciences, Sun Yat-sen University, Zhuhai 519082, China; wuys@mail2.sysu.edu.cn (Y.W.); chenylun3@mail.sysu.edu.cn (Y.C.); zhangaoq3@mail.sysu.edu.cn (A.Z.); tuchy@mail2.sysu.edu.cn (C.T.); eeslwb@mail.sysu.edu.cn (W.L.)

² Guangzhou Institute of Tropical and Marine Meteorology, China Meteorological Administration (CMA), Guangzhou 510640, China; zhoums@gd121.cn

* Correspondence: chenshumin@sml-zhuhai.cn; Tel.: +86-137-2670-3047

Abstract: An improved understanding of the environmental factors influencing tropical cyclones (TCs) is vital to enhance the accuracy of forecasting TC intensity. More than half of TCs that were substantially affected by environmental factors were predominantly affected by low-level environmental relative vorticity (hereafter, VOR TCs). In this study, the seasonal variation and related physical features of VOR TCs from 2003–2017 during TC seasons in summer and autumn over the western North Pacific were analyzed. Autumn VOR TCs exhibited the strongest intensity among all TCs over the western North Pacific. The enhanced environmental relative vorticity during the TC intensification period was larger and more favorably distributed for VOR TC development in autumn. The vorticity diagnostic analysis showed that the convergence was the positive source of environmental relative vorticity of VOR TCs, while the contribution of convergence was larger in autumn than in summer. The increased convergence was related to seasonal variation in larger-scale systems, especially the higher environmental pressure gradient, which reflected the larger subtropical high and the compressed East Asian summer monsoon trough in autumn. In addition, the East Asian summer monsoon trough was also somewhat stronger during the intensification period of VOR TCs, especially in autumn.

Keywords: tropical cyclone; intensification; environmental relative vorticity; seasonal variations



Citation: Wu, Y.; Chen, S.; Zhou, M.; Chen, Y.; Zhang, A.; Tu, C.; Li, W. Effects of Environmental Relative Vorticity and Seasonal Variation on Tropical Cyclones over the Western North Pacific. *Atmosphere* **2022**, *13*, 795. <https://doi.org/10.3390/atmos13050795>

Academic Editors: Yineng Li and Xing Wei

Received: 20 April 2022

Accepted: 11 May 2022

Published: 13 May 2022

Publisher's Note: MDPI stays neutral with regard to jurisdictional claims in published maps and institutional affiliations.



Copyright: © 2022 by the authors. Licensee MDPI, Basel, Switzerland. This article is an open access article distributed under the terms and conditions of the Creative Commons Attribution (CC BY) license (<https://creativecommons.org/licenses/by/4.0/>).

1. Introduction

Tropical cyclones (TCs), which develop over warm tropical oceans, are one of the most serious natural disasters, especially for coastal regions in the western North Pacific (e.g., Japan, Korea, China, and the Philippines) [1–3]. Forecasting skills for TC intensity have remained largely static in recent decades, e.g., [4,5]. This is a result of incomplete comprehension of the physical features of TC intensification. A TC is a complex system, the intensity of which is affected by various internal and environmental factors that interact with underlying physical processes on various scales [6–8]. Increasing the understanding of the environmental factors affecting TCs is one of the most effective ways to improve the ability to forecast TC intensity. According to previous studies, the following environmental factors are considered favorable for TC intensification: small vertical wind shear [9,10], high low-level vorticity [9,11], high upper-level divergence [12,13], high sea surface temperature [14,15], high water vapor content of the troposphere [16,17], and large amounts of convective available potential energy [18,19].

Building on these previous studies, Wu et al. [20] (hereafter, WU20) quantified the contributions of different environmental factors to 181 TCs that were active over the western North Pacific during July–October of 2003–2017 for the entire intensification period. The estimation was based on the stepwise multiple regression method, which

is effective for solving collinearity problems (detailed in Text S1) [21,22]. Environmental factors considered in the estimation included vertical wind shear, low-level relative vorticity, upper-level divergence, sea surface temperature, water vapor content of the troposphere, and convective available potential energy. The estimation results showed that over 70% of the TCs studied were substantially affected by the different environmental factors listed above (hereafter, Environmental TCs). The definition of Environmental TCs is also detailed in Text S2. Moreover, over half of the Environmental TCs were affected predominantly by low-level environmental relative vorticity (hereafter, VOR TCs), while only approximately 4% of the Environmental TCs were affected predominantly by sea surface temperature. This result is largely consistent with the findings of Chan [23], who reported that TCs over the western North Pacific are generally affected by dynamic factors, whereas TCs over the Atlantic are primarily affected by thermodynamic factors. Thus, low-level relative vorticity is considered the primary environmental factor influencing TC intensification over the western North Pacific during the analysis period. In addition, the intensity of VOR TCs was stronger than that of other Environmental TCs, which was in turn stronger than that of TCs unaffected by the selected environmental factors.

Seasonal variation in TCs is governed mainly by large-scale atmospheric or oceanic systems and is one of the major features of TCs (especially regarding their occurrence frequency and intensity); it has attracted considerable research attention in recent years, e.g., [24–26]. For TCs over the western North Pacific, the relevant major large-scale atmospheric systems are the subtropical high and the East Asian summer monsoon trough [10,27]. The East Asian summer monsoon exhibits marked seasonal variation, systematically extending northward in summer and retreating southward in autumn [28,29]. As reported in WU20, low-level divergence and convergence represent the vorticity source for VOR TCs over the western North Pacific and are primarily related to the subtropical high and East Asian summer monsoon trough, respectively. Thus, seasonal variations in VOR TCs during summer and autumn are deserving of further detailed analysis.

Following WU20, the present study analyzed the seasonal (summer–autumn) variation in VOR TCs and associated their physical features using the vorticity equation. The remainder of this paper is organized as follows: Section 2 introduces the data and methods used, including the physical terms of the vorticity equation. Section 3 describes the results derived from the analysis, including the contributions of different physical terms to the environmental vorticity, as well as related large-scale features and their seasonal variation. Section 4 includes a discussion and recommends directions for future work based on the analysis results. Finally, a summary of the study and its conclusions are presented in Section 5.

2. Materials and Methods

Based on WU20, 68 VOR TCs were analyzed during summer (July–August) and autumn (September–October) over a 15-year period (2003–2017). The names and duration of intensification stage for each VOR TC are listed in Table S1. The definition of VOR TC is detailed in Text S2. The European Center for Medium-Range Weather Forecasts ERA-Interim daily dataset, with a horizontal resolution of $1^\circ \times 1^\circ$ and 37 vertical levels [30], was used for the analysis, along with the 6-hourly TC best-track data provided by the Shanghai Typhoon Institute of China Meteorological Administration [31]. The TC intensification period was defined as the point when the minimum central pressure of a TC decreased with time, based on the best-track data. The TC analysis intensification period generally extends from the initiation of the TC to the time of its maximum intensity. The smaller-scale features of each TC were removed according to the filtering method of Kurihara et al. [32,33], and only the large-scale environmental fields were preserved for analysis.

For the vorticity diagnostic analysis, we focused primarily on the annular region from 2° – 8° to the center of the TC, which previous studies have identified as the area constituting a reasonable environmental field for most dynamic and thermodynamic variables (e.g., [34,35]), and the eyewall size in most of the studied TCs generally did

not exceed 200 km. Therefore, the filtered variables within the annular region of 2°–8° from the TC center were analyzed using the vorticity equation, which can be expressed in terms of P-coordinates by ignoring friction as follows:

$$\frac{\partial \zeta}{\partial t} = -\left(u \frac{\partial \zeta}{\partial x} + v \frac{\partial \zeta}{\partial y}\right) - \omega \frac{\partial \zeta}{\partial p} - v \frac{\partial f}{\partial y} - \zeta \left(\frac{\partial u}{\partial x} + \frac{\partial v}{\partial y}\right) - f \left(\frac{\partial u}{\partial x} + \frac{\partial v}{\partial y}\right) + \left(\frac{\partial \omega}{\partial y} \frac{\partial u}{\partial p} - \frac{\partial \omega}{\partial x} \frac{\partial v}{\partial p}\right) + Res. \quad (1)$$

where ζ is relative vorticity; u and v are the zonal and meridional, respectively; ω is the vertical pressure velocity; $-\left(u \frac{\partial \zeta}{\partial x} + v \frac{\partial \zeta}{\partial y}\right)$ is the horizontal advection term (HAT); $-\omega \frac{\partial \zeta}{\partial p}$ is the vertical advection term (VAT); $-v \frac{\partial f}{\partial y}$ is the geostrophic vorticity term (GVT); $-\zeta \left(\frac{\partial u}{\partial x} + \frac{\partial v}{\partial y}\right)$ is the vorticity divergence term (VDT); $-f \left(\frac{\partial u}{\partial x} + \frac{\partial v}{\partial y}\right)$ is the Coriolis vorticity divergence term (CDT); $\left(\frac{\partial \omega}{\partial y} \frac{\partial u}{\partial p} - \frac{\partial \omega}{\partial x} \frac{\partial v}{\partial p}\right)$ represents the tilt term (TT); and finally, *Res.* represents the residual associated with other processes that primarily include the higher nonlinear terms. In the following sections, the differences between VOR TCs and Environmental TCs are analyzed. These differences are referenced as Δ HAT, Δ VAT, Δ GVT, Δ VDT, Δ CDT, Δ TT, and Δ Res. for HAT, VAT, GVT, VDT, CDT, TT, and *Res.*, respectively. The abbreviations defined above are also listed in Appendix A.

3. Results

3.1. Seasonal Variation in Analysis Results Based on the Vorticity Equation

The autumn VOR TCs had the strongest intensity over the western North Pacific of all the TCs studied during the analysis period. Figure 1 shows the seasonal variation present in the intensities of different TCs, represented by the average minimum sea level pressure. VOR TCs were stronger (~5.27 hPa deeper) than Environmental TCs, which were in turn stronger (~15.70 hPa deeper) than the TCs unaffected by environmental factors. All autumn TCs were stronger than summer TCs, and the autumn VOR TCs were approximately 6.52 hPa deeper than summer VOR TCs. The proportion of VOR TCs in autumn was also higher than in summer (Figure 2). Overall, 36 (~59%) of the 61 Environmental TCs that occurred in autumn were VOR TCs; this proportion is approximately 12% larger than that in summer.

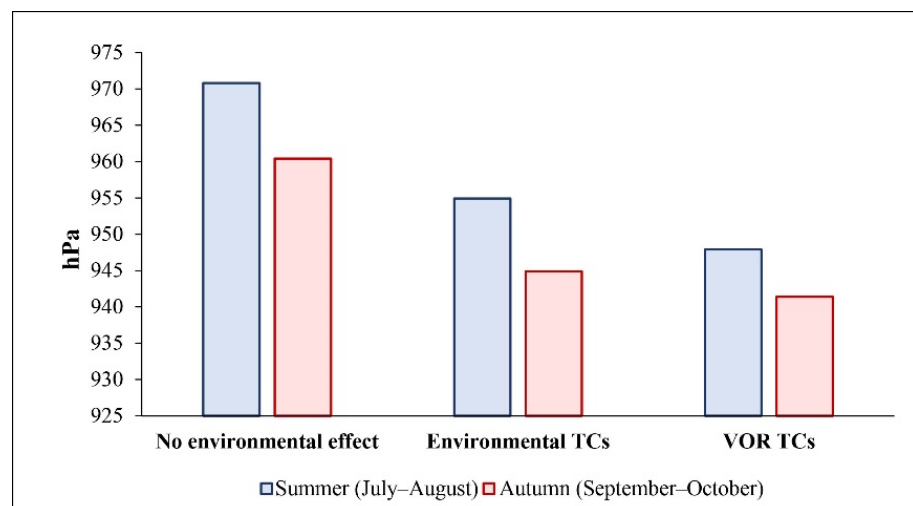


Figure 1. Average minimum sea level pressure of TCs not affected substantially by environmental factors (“No environmental effect”), Environmental TCs, and VOR TCs in summer (July–August) and autumn (September–October).

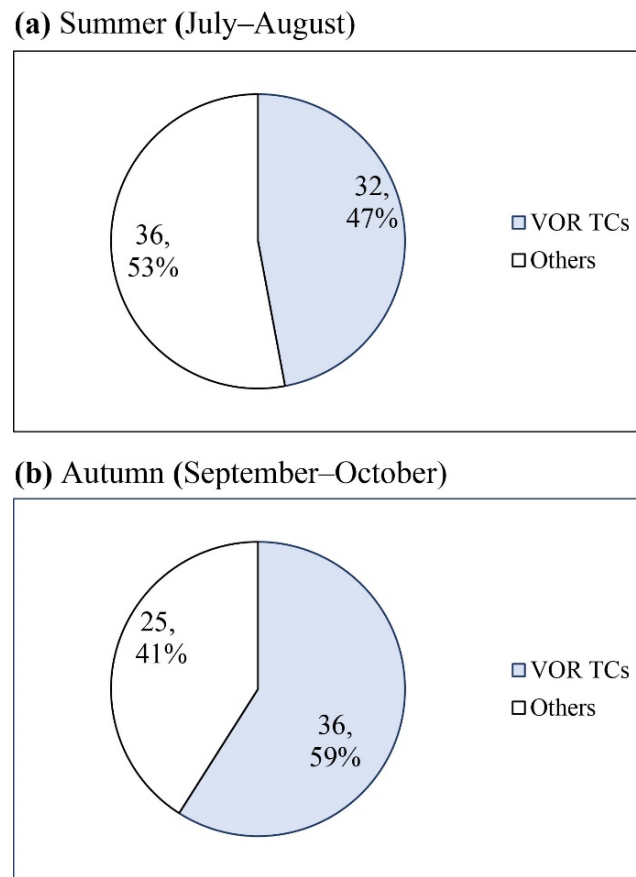


Figure 2. Proportions of VOR TCs (blue) and other Environmental TCs (white) to all Environmental TCs: (a) TCs in summer (July–August) and (b) TCs in autumn (September–October) from 2003–2017.

The distribution of enhanced environmental relative vorticity during the TC intensification period was more favorable for the development of VOR TCs in autumn than in summer (Figure 3). The enhanced environmental relative vorticity during the TC intensification period can be estimated by subtracting the values of environmental relative vorticity when TC began to intensify from the values of environmental relative vorticity when TC reached its maximum intensity. The mean value of enhanced environmental relative vorticity at 850 hPa within the 8° area of the VOR TCs was $5.66 \times 10^{-6} \text{ s}^{-1}$ in autumn, larger than that in summer ($5.26 \times 10^{-6} \text{ s}^{-1}$). Generally, the center of the enhanced environmental relative vorticity was closer to the center of the TC in autumn, whereas it was approximately 1° south and 2° west of the TC center in summer. The distribution of the environmental relative vorticity was also more homogeneous in autumn than in summer. In autumn, the mean value of the southern part ($7.91 \times 10^{-6} \text{ s}^{-1}$) was approximately twice that of the northern region ($3.41 \times 10^{-6} \text{ s}^{-1}$). In summer, the mean value of the southern part ($8.51 \times 10^{-6} \text{ s}^{-1}$) was approximately four times that of the northern part ($2.0 \times 10^{-6} \text{ s}^{-1}$), and the values in the southwestern part were also obviously larger than those in the southeastern part. The enhanced environmental relative vorticity during the VOR TC intensification period was larger than that of all Environmental TCs (including VOR TCs); additionally, the difference between them was larger in autumn ($2.39 \times 10^{-6} \text{ s}^{-1}$) than in summer ($2.08 \times 10^{-6} \text{ s}^{-1}$) (Figure 4). The largest difference occurred in the southwestern (southern) part of TC in summer (autumn). The fact that the enhanced environmental relative vorticity during the VOR TC intensification period was larger in autumn than in summer is attributable to the combined effect of the subtropical high and East Asian summer monsoon trough, which is discussed further in Section 3.2.

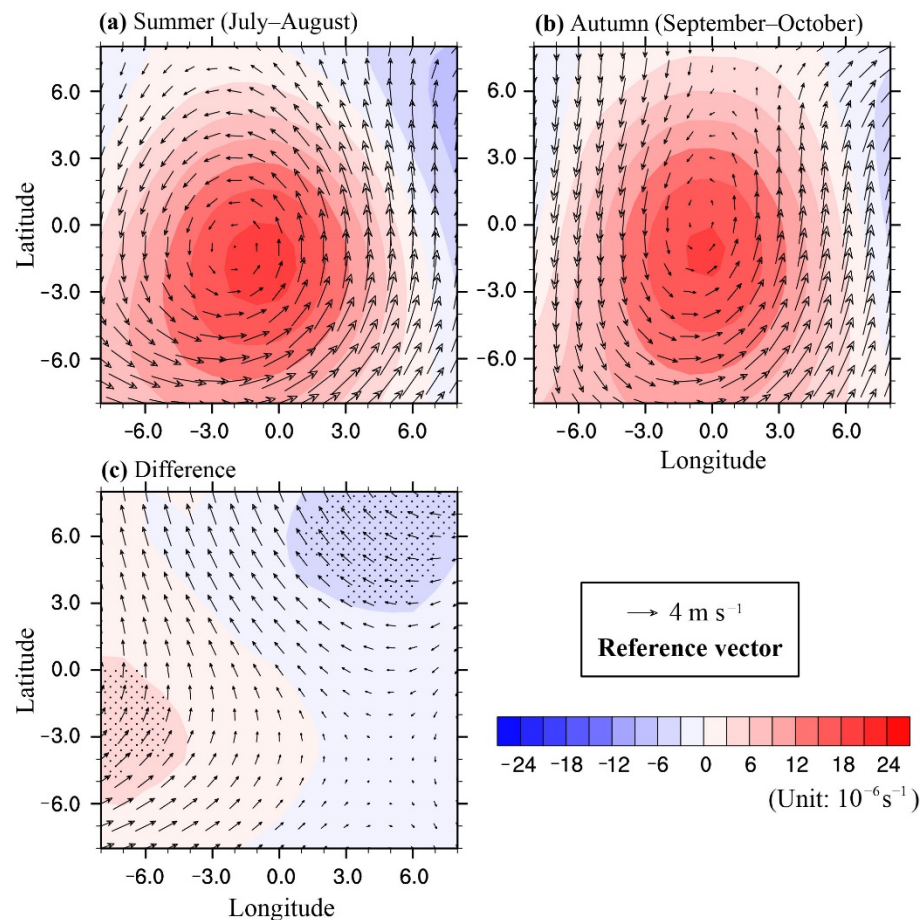


Figure 3. Average enhanced environmental relative vorticity (shading; unit: 10^{-6} s^{-1}) and enhanced environmental wind vectors (unit: m s^{-1}) at 850 hPa, during intensification stage of VOR TCs, of the area of approximately 8° longitude/latitude around the TC center. Zero coordinates (0, 0) indicate the location of the TC center. Here, smaller-scale features of variables related to the TC structure were removed based on the filtering method of Kurihara et al. [32,33]: (a) TCs in summer (July–August), (b) TCs in autumn (September–October), and (c) differences between summer and autumn. Dots in (c) indicate areas of $>90\%$ confidence level according to the Student's t -test.

3.2. Seasonal Variation in Analysis Results Based on the Vorticity Equation

Based on the vorticity diagnosis analysis for the fields at 850 hPa in the annular region of 2° – 8° from the center of the VOR TCs using Equation (1), the environmental relative vorticity was found to be more favorable in autumn than in summer for VOR TC development (Figure 5a). The mean environmental vorticity tendency ($\frac{\partial \zeta}{\partial t}$) in autumn ($2.38 \times 10^{-11} \text{ s}^{-2}$) was approximately twice that in summer ($1.20 \times 10^{-11} \text{ s}^{-2}$), corresponding to the larger enhanced environmental relative vorticity during the VOR TC intensification period in autumn compared to that in summer. The Coriolis vorticity and vorticity divergence terms (CDT and VDT, respectively) were the main sources of environmental vorticity for VOR TCs in both summer and autumn, whereas the contributions of the other terms were negative or relatively small. The CDT and VDT of VOR TCs (5.88×10^{-11} and $1.55 \times 10^{-11} \text{ s}^{-2}$, respectively) were 0.52×10^{-11} and $0.45 \times 10^{-11} \text{ s}^{-2}$ larger in autumn than in summer, respectively. The geostrophic vorticity term (GVT) and the horizontal advection term (HAT) were the two main negative terms for VOR TCs. The values of HAT were similar in summer ($-1.26 \times 10^{-11} \text{ s}^{-2}$) and autumn ($-1.43 \times 10^{-11} \text{ s}^{-2}$), whereas the absolute value of the GVT in summer ($-4.35 \times 10^{-11} \text{ s}^{-2}$) was $1.11 \times 10^{-11} \text{ s}^{-2}$ larger than that in autumn.

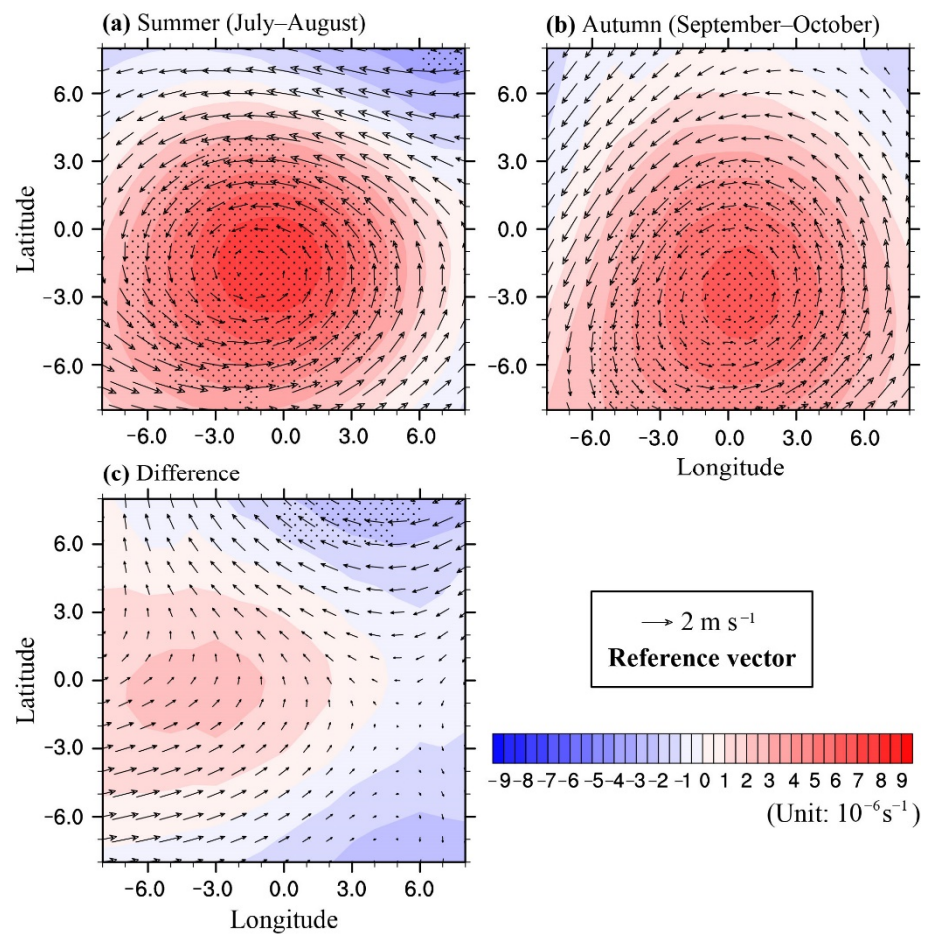


Figure 4. Difference of average enhanced environmental relative vorticity (shading; unit: 10^{-6} s^{-1}) and enhanced environmental wind vectors (unit: m s^{-1}) at 850 hPa between VOR TCs and all Environmental TCs, during intensification stage of VOR TCs, of the area of approximately 8° longitude/latitude around the TC center. Zero coordinates (0, 0) indicate the location of the TC center. Here, smaller-scale features of variables related to the TC structure were removed based on the filtering method of Kurihara et al. [32,33]: (a) TCs in summer (July–August), (b) TCs in autumn (September–October), and (c) differences between summer and autumn. Dots in (c) indicate areas of $>90\%$ confidence level according to the Student's t -test.

The differences between the terms of the vorticity equation (Equation (1)) for VOR TCs and Environmental TCs show that the environmental conditions were more favorable for VOR TCs in autumn than in summer (Figure 5b). The value of the difference in the mean environmental vorticity tendency ($\frac{\partial \zeta}{\partial t}$) (ΔVOR tendency) in autumn ($0.47 \times 10^{-11} \text{ s}^{-2}$) was $0.14 \times 10^{-11} \text{ s}^{-2}$ larger than in summer. This also corresponded to the larger difference in enhanced environmental relative vorticity during the VOR intensification period in autumn compared to that in summer. The difference in the horizontal advection term (ΔHAT) was similar for the two seasons, with values of $-0.33 \times 10^{-11} \text{ s}^{-2}$ in summer and $-0.29 \times 10^{-11} \text{ s}^{-2}$ in autumn. In autumn, the differences in the vorticity and Coriolis vorticity divergence terms (ΔVDT and ΔCDT , respectively) also made positive contributions to the ΔVOR tendency, with values of 0.37×10^{-11} and $0.70 \times 10^{-11} \text{ s}^{-2}$, respectively. However, the values of VDT and CDT between VOR TCs and Environmental TCs were not significant in summer; thus, the values of ΔVDT and ΔCDT were neglected. In contrast to autumn, the contribution of the difference in the geostrophic vorticity term (ΔGVDT) was positive in summer ($0.60 \times 10^{-11} \text{ s}^{-2}$), which contributed to a vorticity environment that was more favorable for the development of VOR TCs than for other Environmental TCs during this season.

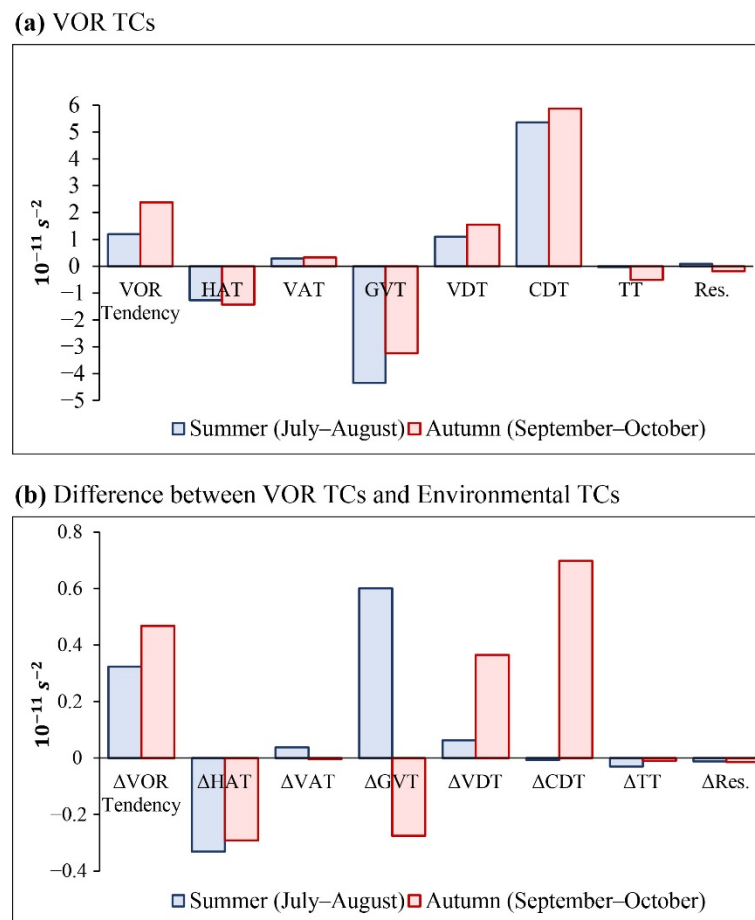


Figure 5. Different terms (unit: $10^{-11} s^{-2}$) in the vorticity equation at 850 hPa, averaged within the annulus area of 2° – 8° from the TC center during the intensification period: (a) VOR TCs and (b) difference between VOR TCs and Environmental TCs. In (a), VOR Tendency means the vorticity tendency ($\frac{\partial \zeta}{\partial t}$) for VOR TCs; in (b), Δ VOR Tendency means $\frac{\partial \zeta}{\partial t}$ for the difference between VOR TCs and Environmental TCs.

3.3. Physical Links to Seasonal Variation in Large-Scale Atmospheric Systems

The higher contributions of the vorticity and Coriolis vorticity divergence terms (e.g., $CDT/\Delta CDT$ and $VDT/\Delta VDT$) in autumn were related to the greater convergence, which was generally controlled by large-scale systems over the western North Pacific, e.g., the subtropical high and East Asian summer monsoon trough. The TCs were most active in the East Asian summer monsoon trough region (Figure 6). The monsoon trough was stronger in summer than in autumn, e.g., during the Environmental TC intensification period. The area of the East Asian summer monsoon trough was larger in summer than in autumn, as indicated by the 1490 gpm contour extending from approximately 10° N to around 28° N (Figure 6a). The monsoon trough retreated and became smaller in autumn, as shown by the reduced extent of the 1490 gpm contour (10 – 21° N), and the 1480 gpm contour became compressed into an isolated closed low system (Figure 6b). The autumn subtropical high was enlarged, although its intensity was not as strong as in summer, where it had the highest contour of 1570 gpm, e.g., approximately 30 gpm higher than in autumn. The compressed area of the monsoon trough and enlarged area of the subtropical high in autumn contributed to the enhanced convergence via the higher pressure gradient around the TCs, which then generated a larger CDT and VDT in autumn than in summer. During the summer VOR TC intensification period, the monsoon trough was strengthened and extended to the region of the mean subtropical high; e.g., many values that passed the $>90\%$ confidence level appeared within the area indicated as >1520 gpm (Figure 6a).

As a result of the combined effect of the low-level convergence and divergence generated by the enhanced monsoon trough and mean subtropical high, respectively, the difference in divergence between VOR TCs and Environmental TCs was not significant in summer (Figure 7a). This contributed to the small Δ CDT and Δ VDT values in summer. During the autumn VOR TC intensification period, the low monsoon area was also intensified, but it did not extend to the subtropical high; e.g., no values that passed the >90% confidence level appeared in the area indicated as >1520 gpm. Thus, the convergence around the VOR TCs was substantially greater than that around the Environmental TCs (Figure 7b), which contributed to the larger Δ CDT and Δ VDT in autumn compared to those of the Environmental TCs.

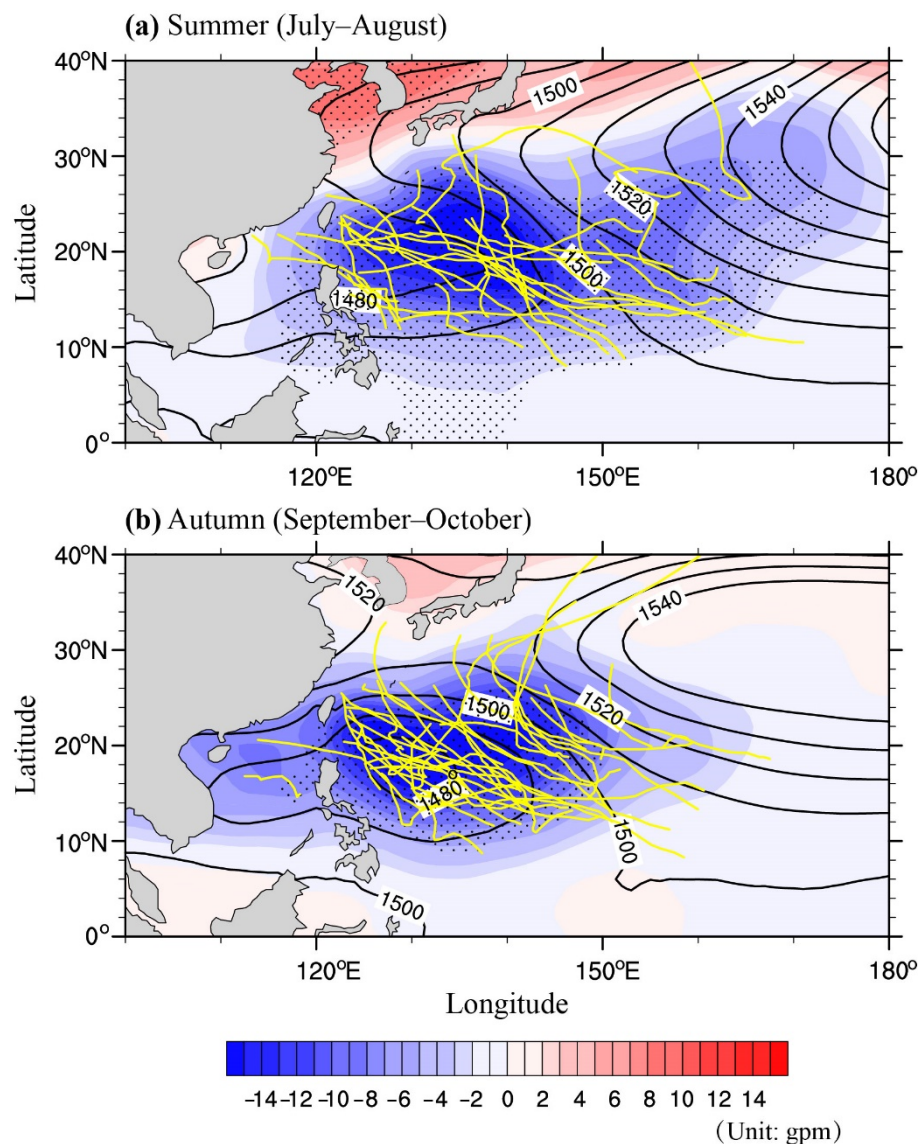


Figure 6. Composite geopotential height of Environmental TCs (contours; unit: gpm) and its difference between VOR TCs and Environmental TCs (shading; unit: gpm) at 850 hPa. Dots indicate areas of >90% confidence level according to the Student’s *t*-test for the difference between VOR TCs and Environmental TCs. The yellow lines indicate the tracks of VOR TCs during their intensification period: (a) TCs in summer (July–August) and (b) TCs in autumn (September–October).

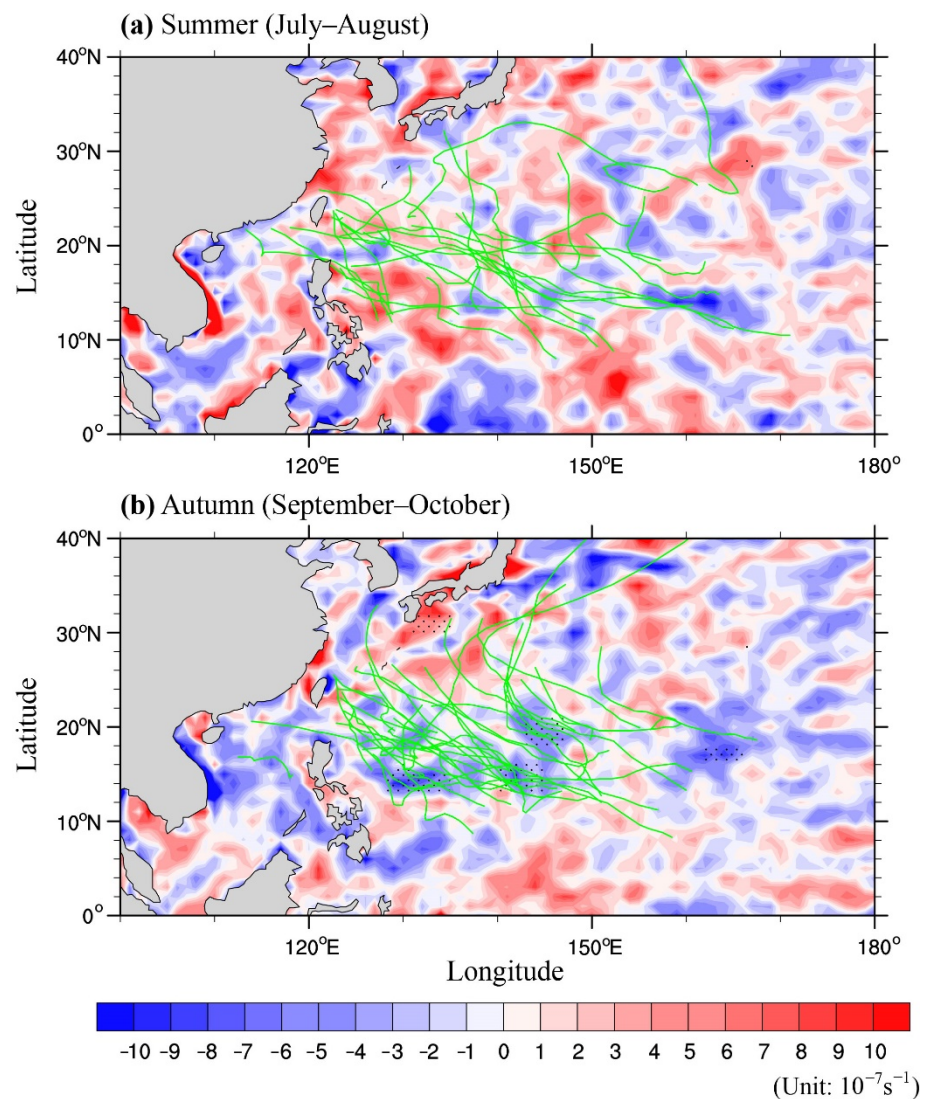


Figure 7. Difference of composite divergence (shading; unit: 10^{-7} s^{-1}) between VOR TCs and Environmental TCs at 850 hPa. Dots indicate areas of >90% confidence level according to the Student's *t*-test. The green lines indicate the tracks of VOR TCs during their intensification period: (a) TCs in summer (July–August) and (b) TCs in autumn (September–October).

The contribution of the difference in the geostrophic vorticity term (GVT) between VOR TCs and Environmental TCs (ΔGVT) showed the largest difference between summer and autumn, and the seasonal variations in ΔGVT and GVT were also responses to the subtropical high and East Asian summer monsoon trough. Because the values of $\partial f/\partial y$ were positive and generally similar for all analyzed TCs, the values of GVT (ΔGVT) ($-v \partial f/\partial y$) were governed by the values of the opposite direction of meridional winds ($-v$). Thus, the negative contribution of the GVT to VOR TCs was larger in summer than in autumn (Figure 5a) owing to the weaker environmental northerly winds on the western side of the TCs (Figure 8). This was caused by the large East Asian summer monsoon trough that was open on its western side in summer, unlike the closed low system area in autumn (Figure 6). Compared to Environmental TCs, the environmental south winds to the east of the VOR TC center on the western side of the subtropical high were weakened, because the subtropical high was weakened by the enlarged monsoon trough. This resulted in large positive mean ΔGVT values (Figure 5b), which were in turn a result of the abnormal northerly winds on the eastern side of the VOR TCs (Figure 9a). Conversely, in comparison with other Environmental TCs, abnormal southerly winds appeared on the eastern side of the autumn VOR TCs. This was because the East Asian summer monsoon trough was intensified but

not enough to weaken the subtropical high compared with the case of Environmental TCs (Figure 9b), which resulted in the negative mean values of Δ GVT in this season (Figure 5b).

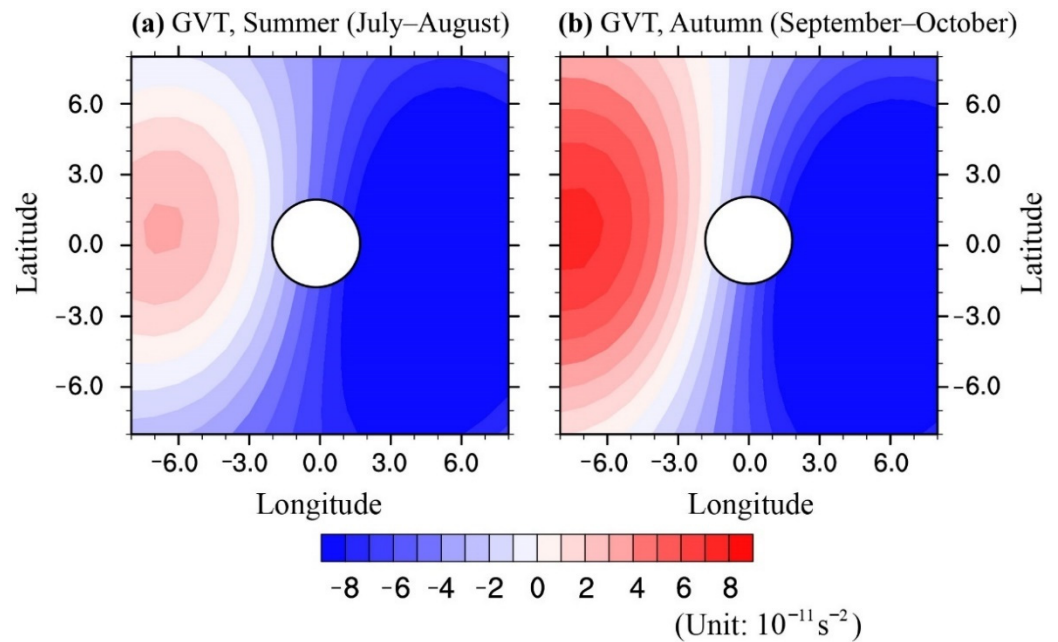


Figure 8. Composite values of the GVT in Equation (1) (shading; unit: 10^{-11} s^{-2}) for VOR TCs. The white circles indicate the region of $<2^\circ$ longitude/latitude from the center of each TC: (a) TCs in summer (July–August) and (b) TCs in autumn (September–October).

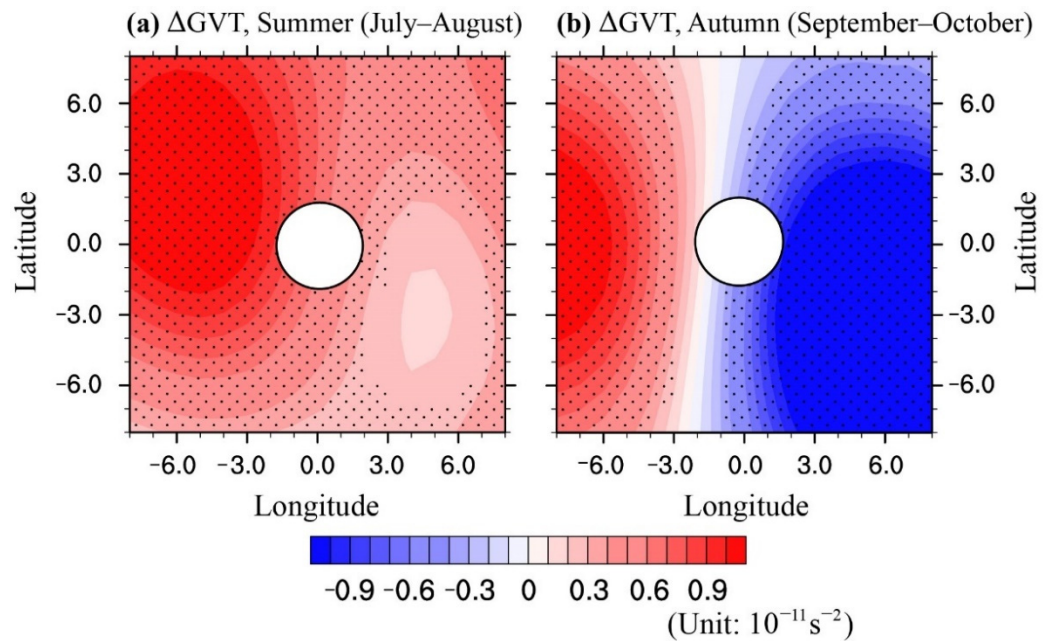


Figure 9. The composite difference in the GVT (Δ GVT) in Equation (1) (shading; unit: 10^{-11} s^{-2}) between VOR TCs and Environmental TCs. The white circles indicate the region of $<2^\circ$ longitude/latitude from the center of each TC: (a) TCs in summer (July–August) and (b) TCs in autumn (September–October).

Notably, the distribution of enhanced environmental relative vorticity (Figures 3 and 4), which was more favorable for the development of VOR TCs in autumn, was also a contribution of the weakened East Asian summer monsoon trough. The larger enhanced vorticity in autumn, with its center nearer to the TC center than in summer, was possibly a

contribution of the compressed East Asian summer monsoon trough, which concentrated more environmental vorticity in the TC region (Figure 6). In summer, as a result of the enhanced East Asian summer monsoon trough, which extended to the western side of the subtropical high, a larger difference in enhanced environmental relative vorticity between VOR TCs and Environmental TCs occurred in the southwestern part of the TCs (Figure 4).

4. Discussion

Another possible reason for the larger proportion of VOR TCs during autumn is that the thermodynamic factors in summer are more favorable for TC development than in autumn. The proportion of TCs affected by thermodynamic and dynamic factors during the two seasons is shown in Figure 10. Details of the TC numbers are listed in Table 1 and are organized according to the classification structure described by Chan [23]. Overall, approximately 37% of summer TCs (approximately 11% more than in autumn) were affected by thermodynamic factors. Based on observational records (e.g., [36,37]), compared to the other seasons, the summertime atmospheric thermodynamic conduction over the western North Pacific contains more heat and water vapor, providing conditions favorable for TC development. Thus, detailed physical analysis of the thermodynamic processes related to summer TCs is required.

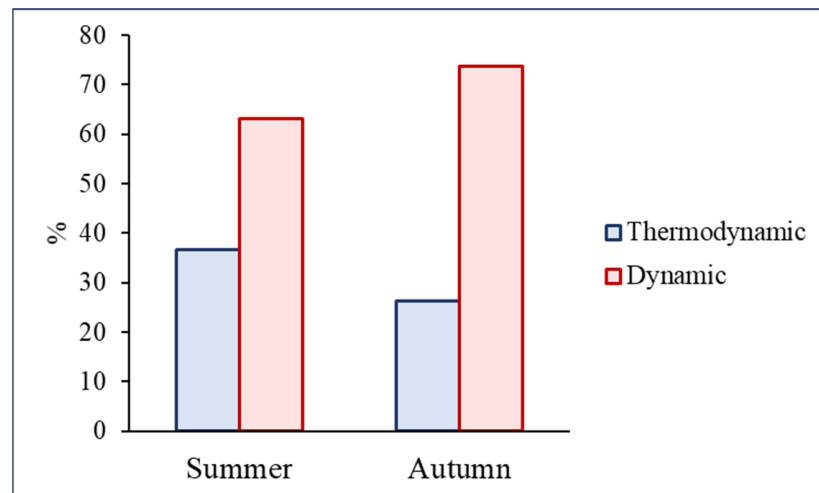


Figure 10. Proportions of TCs affected predominantly by thermodynamic and dynamic factors during summer (July–August) and autumn (September–October). The estimation was based on the statistical results of WU20, which are also listed in Table 1.

Table 1. Numbers of TCs affected predominantly by different factors ¹.

	Summer (July–August)	Autumn (September–October)
Q TCs (thermodynamic)	13	8
CAPE TCs (thermodynamic)	9	6
SST TCs (thermodynamic)	3	2
VOR TCs (dynamic)	32	36
VWS TCs (dynamic)	7	5
DIV TCs (dynamic)	4	4

¹ The meanings of the abbreviations are listed in Appendix A.

5. Conclusions

Of all of the TCs occurring over the western North Pacific during the analysis period, the autumn VOR TCs exhibited the strongest intensity. The proportion of VOR TCs to Environmental TCs was also larger in autumn than in summer. Analysis results based on the vorticity equation (Equation (1)) showed that the environmental relative vorticity in autumn was more favorable for the development of VOR TCs than that in summer, with the mean environmental vorticity tendency in autumn ($2.38 \times 10^{-11} \text{ s}^{-2}$) being approximately

twice that in summer ($1.20 \times 10^{-11} \text{ s}^{-2}$). The Coriolis vorticity divergence and vorticity divergence terms (e.g., $\text{CDT}/\Delta\text{CDT}$ and $\text{VDT}/\Delta\text{VDT}$) were the principal sources of the environmental relative vorticity of VOR TCs in both seasons, and their contribution was larger in autumn than in summer. The geostrophic vorticity and horizontal advection terms (GVT and HAT, respectively) were the two main negative terms; the other terms were relatively small and so were neglected. Unlike autumn, the difference in GVT between VOR TCs and Environmental TCs (ΔGVT) made a positive contribution in summer, creating a vorticity environment that was more favorable for the development of VOR TCs than for other Environmental TCs.

The higher contributions of the terms related to vorticity convergence (e.g., $\text{CDT}/\Delta\text{CDT}$ and $\text{VDT}/\Delta\text{VDT}$) in autumn were related to the larger convergence, which was controlled by the seasonal variation in the subtropical high, in combination with the East Asian summer monsoon trough over the western North Pacific. In autumn, the monsoon trough retreated and decreased in size, while the area of the subtropical high increased, although its intensity was weaker in summer. Thus, the larger convergence was generated as a result of the greater pressure gradient contributed by the compressed monsoon trough and an enlarged subtropical high, which then contributed to the larger CDT and VDT around the VOR TCs in comparison with those in summer. Seasonal variations in the geostrophic vorticity term ($\text{GVT}/\Delta\text{GVT}$) were also a response to the subtropical high and East Asian summer monsoon trough. In summer, the larger and stronger East Asian summer monsoon trough extended further northeastward, which weakened the western side of the subtropical high and generated weaker environmental southerly winds on the eastern side of the TCs. This resulted in a smaller negative contribution of the GVT to VOR TCs (in comparison with Environmental TCs) in summer than in autumn, while a positive value of the ΔGVT was observed.

Moreover, another possible reason for the larger proportion of VOR TCs during autumn is that thermodynamic factors are more favorable for TC development in summer, as seen in observational records. Finally, VOR TCs that usually exhibit a higher intensity are related to a stronger East Asian summer monsoon trough; therefore, a strong monsoon trough may indicate the development of severe TCs via practical forecasting, especially in autumn.

Supplementary Materials: The following supporting information can be downloaded at: <https://www.mdpi.com/article/10.3390/atmos13050795/s1>, Table S1: Names and duration of analyzed VOR TCs in summer (July–August) and autumn (September–October); Text S1: Introduction of the stepwise multiple regression method; Text S2: Definition of Environmental TC and VOR TC.

Author Contributions: Conceptualization, S.C. and W.L.; methodology, M.Z.; formal analysis, Y.W.; investigation, Y.W.; resources, A.Z., Y.C., and C.T.; writing—original draft preparation, S.C.; writing—review and editing, S.C.; supervision, S.C.; project administration, S.C.; funding acquisition, W.L. All authors have read and agreed to the published version of the manuscript.

Funding: This work research was funded by the Key Research and Development Projects in Guangdong Province, grant number 2019B111101002, Fundamental Research Funds for the Guangzhou Science and Technology Plan Project, grant number 201903010036, National Natural Science Foundation of China, grant numbers 42105068, 42075004, 42005062, and 42075086, and Guangdong Basic and Applied Basic Research Foundation, grant number 2022A1515011100.

Data Availability Statement: Shanghai Typhoon Institute of China Meteorological Administration [31]. Available online: <http://tcdata.typhoon.org.cn> (accessed on 19 April 2022). European Center for Medium-Range Weather Forecasts [30]. Available online: <https://www.ecmwf.int/en/forecasts/datasets/archive-datasets/reanalysis-datasets/era-interim> (accessed on 19 April 2022).

Acknowledgments: We thank James Buxton, MSc, from Liwen Bianji, Edanz Group China (<https://en-author-services.edanzgroup.com/ac> (accessed on 19 April 2022)), for editing the English text of this manuscript.

Conflicts of Interest: The authors declare no conflict of interest.

Appendix A

Explanations of the abbreviations

TC: tropical cyclone.

WU20: Wu, Y.; Chen, S.; Li, W.; Fang, R.; Liu, H.; Relative vorticity is the major environmental factor controlling tropical cyclone intensification over the western North Pacific. *Atmos. Res.* **2020**, *237*(2020), 104874. DOI: 10.1016/j.atmosres.2020.104874.

MCP: minimum central pressure of a TC.

Environmental TC: a TC for which intensification was affected significantly by environmental factors.

VWS TC: a TC for which intensification was affected predominantly by environmental vertical wind shear (VWS).

VOR TC: a TC for which intensification was affected predominantly by low-level environmental relative vorticity (VOR).

DIV TC: a TC for which intensification was affected predominantly by environmental upper-level divergence (DIV).

Q TC: a TC for which intensification was affected predominantly by the environmental water vapor content of the troposphere (Q).

SST TC: a TC for which intensification was affected predominantly by sea surface temperature (SST).

CAPE TC: a TC for which intensification was affected predominantly by environmental convective available potential energy (CAPE).

Abbreviations for terms in the vorticity diagnostic equation:

VOR Tendency: tendency of the relative vorticity, $\frac{\partial \zeta}{\partial t}$.

Δ VOR Tendency: difference in the VOR Tendency between a VOR TC and an Environmental TC.

HAT: horizontal advection term, $-\left(u \frac{\partial \zeta}{\partial x} + v \frac{\partial \zeta}{\partial y}\right)$.

Δ HAT: difference in the HAT between a VOR TC and an Environmental TC.

VAT: vertical advection term, $-\omega \frac{\partial \zeta}{\partial p}$.

Δ VAT: difference in the VAT between a VOR TC and an Environmental TC.

GVT: geostrophic vorticity term, $-v \frac{\partial f}{\partial y}$.

Δ GVT: difference in the GVT between a VOR TC and an Environmental TC.

VDT: vorticity divergence term, $-\zeta \left(\frac{\partial u}{\partial x} + \frac{\partial v}{\partial y}\right)$.

Δ VDT: difference in the VDT between a VOR TC and an Environmental TC.

CDT: Coriolis vorticity divergence term, $-f \left(\frac{\partial u}{\partial x} + \frac{\partial v}{\partial y}\right)$.

Δ CDT: difference in the CDT between a VOR TC and an Environmental TC.

TT: tilt term, $\left(\frac{\partial \omega}{\partial y} \frac{\partial u}{\partial p} - \frac{\partial \omega}{\partial x} \frac{\partial v}{\partial p}\right)$.

Δ TT: difference in the TT between a VOR TC and an Environmental TC.

Res.: residual.

Δ Res.: difference in the Res. between a VOR TC and an Environmental TC.

References

1. Gaona, M.F.R.; Villarini, G.; Zhang, W.; Vecchi, G. The added value of IMERG in characterizing rainfall in tropical cyclones. *Atmos. Res.* **2018**, *209*, 95–102. [[CrossRef](#)]
2. Zhou, Y.; Matyas, C.; Li, H.; Tang, J. 2018: Conditions associated with rain field size for tropical cyclones landfalling over the Eastern United States. *Atmos. Res.* **2018**, *214*, 375–385. [[CrossRef](#)]
3. Chen, A.; Ho, C.H.; Chen, D.; Azorin-Molina, C. Tropical cyclone rainfall in the Mekong River Basin for 1983–2016. *Atmos. Res.* **2019**, *226*, 66–75. [[CrossRef](#)]
4. DeMaria, M.; Sampson, C.R.; Knaff, J.A.; Musgrave, K.D. Is tropical cyclone intensity guidance improving? *Bull. Amer. Meteor. Soc.* **2014**, *95*, 387–398. [[CrossRef](#)]
5. Courtney, J.B.; Langlade, S.; Sampson, C.R.; Knaff, J.A.; Birchard, T.; Barlow, S.; Kotal, S.D.; Kriat, T.; Lee, W.; Pasch, R.; et al. Operational perspectives on tropical cyclone intensity change part 1: Recent advances in intensity guidance. *Trop. Cyclone Res. Rev.* **2019**, *8*, 123–133. [[CrossRef](#)]
6. Hendricks, E.A. Internal dynamical control on tropical cyclone intensity variability—a review. *Trop. Cyclone Res. Rev.* **2012**, *1*, 72–78. [[CrossRef](#)]

7. Khain, A.; Lynn, B.; Shpund, J. High resolution WRF simulations of Hurricane Irene: Sensitivity to aerosols and choice of microphysical schemes. *Atmos. Res.* **2016**, *167*, 129–145. [[CrossRef](#)]
8. Leroux, M.D.; Wood, K.; Elsberry, R.L.; Cayan, E.; Hendricks, E.; Kucas, M.; Otto, P.; Rogers, R.; Sampson, B.; Yu, Z. Recent advances in research and forecasting of tropical cyclone track, intensity, and structure at landfall. *Trop. Cyclone Res. Rev.* **2018**, *7*, 85–105. [[CrossRef](#)]
9. Chen, X.; Wang, Y.; Zhao, K. Synoptic flow patterns and large-scale characteristics associated with rapidly intensifying tropical cyclones in the South China Sea. *Mon. Wea. Rev.* **2015**, *143*, 64–87. [[CrossRef](#)]
10. Wang, C.; Wu, L. Future changes of the monsoon trough: Sensitivity to sea surface temperature gradient and implications for tropical cyclone activity. *Earth's Future* **2018**, *6*, 919–936. [[CrossRef](#)]
11. Chan, J.C.L. Comment on “Changes in tropical cyclone number, duration, and intensity in a warming environment”. *Science* **2006**, *311*, 1713. [[CrossRef](#)] [[PubMed](#)]
12. Bosart, L.F.; Bracken, W.E.; Molinari, J.; Velden, C.S.; Black, P.G. Environmental influences on the rapid intensification of Hurricane Opal (1995) over the Gulf of Mexico. *Mon. Wea. Rev.* **2000**, *128*, 322–352. [[CrossRef](#)]
13. Maru, E.; Shibata, T.; Ito, K.J. Statistical analysis of tropical cyclones in the Solomon Islands. *Atmosphere* **2018**, *9*, 227. [[CrossRef](#)]
14. Emanuel, K. The maximum intensity of hurricanes. *J. Atmos. Sci.* **1998**, *45*, 1143–1155. [[CrossRef](#)]
15. Strazzo, S.E.; Elsner, J.B.; LaRow, T.E.; Murakami, H.; Wehner, M.; Zhao, M. The influence of model resolution on the simulated sensitivity of North Atlantic tropical cyclone maximum intensity to sea surface temperature. *J. Adv. Model. Earth. Syst.* **2016**, *8*, 1037–1054. [[CrossRef](#)]
16. Charney, J.G.; Eliassen, A. On the growth of the hurricane depression. *J. Atmos. Sci.* **1964**, *21*, 68–75. [[CrossRef](#)]
17. Kaplan, J.; DeMaria, M. Large-scale characteristics of rapidly intensifying tropical cyclones in the North Atlantic basin. *Wea. Forecast.* **2003**, *18*, 1093–1108. [[CrossRef](#)]
18. Cheung, K.K.W.; Elsberry, R.L. Tropical cyclone formations over the western North Pacific in the Navy Operational Global Atmospheric Prediction System forecasts. *Wea. Forecast.* **2002**, *17*, 800–820. [[CrossRef](#)]
19. Lee, M.; Frisius, T. 2018: On the role of convective available potential energy (CAPE) in tropical cyclone intensification. *Tellus A* **2018**, *70*, 1–18. [[CrossRef](#)]
20. Wu, Y.; Chen, S.; Li, W.; Fang, R.; Liu, H. Relative vorticity is the major environmental factor controlling tropical cyclone intensification over the western North Pacific. *Atmos. Res.* **2020**, *237*, 104874. [[CrossRef](#)]
21. Franc, N.; Götzmark, F.; Økland, B.; Nordén, B.; Paltto, H. Factors and scales potentially important for saproxylic beetles in temperate mixed oak forest. *Biol. Conserv.* **2007**, *135*, 86–98. [[CrossRef](#)]
22. Abudu, S.; Cui, C.; King, J.P.; Moreno, J.; Bawazir, A.S. Modeling of daily pan evaporation using partial least squares regression. *Sci. China. Tech. Sci.* **2010**, *54*, 163–174. [[CrossRef](#)]
23. Chan, J.C.L. Thermodynamic control on the climate of intense tropical cyclones. *Proc. R. Soc. A* **2009**, *465*, 3011–3021. [[CrossRef](#)]
24. Wang, X.; Zhou, W.; Li, C.; Wang, D. Effects of the East Asian summer monsoon on tropical cyclone genesis over the South China Sea on an interdecadal time scale. *Adv. Atmos. Sci.* **2012**, *29*, 249–262. [[CrossRef](#)]
25. Liu, K.S.; Chan, J.C.L. Interannual variation of Southern Hemisphere tropical cyclone activity and seasonal forecast of tropical cyclone number in the Australian region. *Int. J. Climatol.* **2012**, *32*, 190–202. [[CrossRef](#)]
26. Lee, D.K.; Cha, D.H.; Jin, C.S.; Choi, S.J. A regional climate change simulation over East Asia. *Asia-Pac. J. Atmos. Sci.* **2013**, *49*, 655–664. [[CrossRef](#)]
27. Wang, C.; Wang, B. Tropical cyclone predictability shaped by western Pacific subtropical high: Integration of trans-basin sea surface temperature effects. *Clim. Dyn.* **2019**, *53*, 2697–2714. [[CrossRef](#)]
28. Yang, S.; Zhang, Z.; Kousky, V.E.; Higgins, R.W.; Yoo, S.; Liang, J.; Fan, Y. Simulations and seasonal prediction of the Asian Summer Monsoon in the NCEP climate forecast system. *J. Clim.* **2008**, *21*, 3755–3775. [[CrossRef](#)]
29. Fang, Y.; Zhang, Y.; Huang, A.; Li, B. Seasonal and intraseasonal variations of East Asian summer monsoon precipitation simulated by a regional air-sea coupled model. *Adv. Atmos. Sci.* **2013**, *30*, 315–329. [[CrossRef](#)]
30. Dee, D.P.; Uppala, S.M.; Simmons, A.J.; Berrisford, P.; Poli, P.; Kobayashi, S.; Andrae, U.; Balmaseda, M.A.; Balsamo, G.; Bauer, P.; et al. The ERA-Interim reanalysis: Configuration and performance of the data assimilation system. *Q. J. R. Meteorol. Soc.* **2011**, *137*, 553–597. [[CrossRef](#)]
31. Ying, M.; Zhang, W.; Yu, H.; Lu, X.; Feng, J.; Fan, Y.; Zhu, Y.; Chen, D.J. An overview of the China Meteorological Administration tropical cyclone database. *J. Atmos. Ocean. Technol.* **2014**, *31*, 287–301. [[CrossRef](#)]
32. Kurihara, Y.; Bender, M.A.; Tuleya, R.E.; Ross, R.J. Prediction experiments of Hurricane Gloria (1985) using a multiply nested movable mesh model. *Mon. Wea. Rev.* **1990**, *118*, 2185–2198. [[CrossRef](#)]
33. Kurihara, Y.; Bender, M.A.; Ross, R. An initialization scheme of hurricane models by vortex specification. *Mon. Wea. Rev.* **1993**, *121*, 2030–2045. [[CrossRef](#)]
34. Barry, R.G.; Chorley, A.R.J. *Atmosphere, Weather and Climate*, 4th ed.; Methuen: London, UK, 1982; p. 407.
35. Terry, J.P. *Tropical Cyclones*; Springer: New York, NY, USA, 2007; pp. 26–32. [[CrossRef](#)]
36. Liang, C.K.; Eldering, A.; Gettelman, A.; Tian, B.; Wong, S.; Fetzer, E.J.; Liou, K.N. Record of tropical interannual variability of temperature and water vapor from a combined AIRS-MLS data set. *J. Geophys. Res.* **2011**, *116*, D06103. [[CrossRef](#)]
37. Suneeth, K.V.; Das, S.S. Zonally resolved water vapour coupling with tropical tropopause temperature: Seasonal and interannual variability, and influence of the Walker circulation. *Clim. Dyn.* **2020**, *54*, 4657–4673. [[CrossRef](#)]